RSC Advances

ROYAL SOCIETY OF CHEMISTRY

www.rsc.org/advances

TOC Graphic

Nano-Au supported on nanocrystalline $Ce_{0.9}Fe_{0.1}O_{2-\delta}$ solid solution was found to be show excellent catalytic performance for both CO oxidation and benzylamine oxidation.

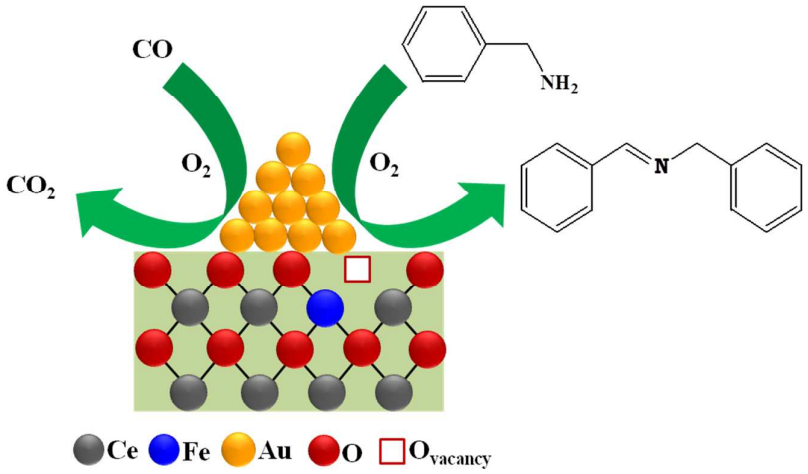

Cite this: DOI: 10.1039/c0xx00000x

www.rsc.org/xxxxxx

ARTICLE TYPE

Structural evaluation and catalytic performance of nano-Au supported on nanocrystalline $Ce_{0.9}Fe_{0.1}O_{2-\delta}$ solid solution for oxidation of carbon monoxide and benzylamine

P. Sudarsanam,[a,b] P. R. Selvakannan,[b] Sarvesh K. Soni,[b] Suresh K. Bhargava,*[b] and Benjaram M. Reddy*[a]

Received (in XXX, XXX) Xth XXXXXXXXX 20XX, Accepted Xth XXXXXXXXX 20XX
DOI: 10.1039/b000000x

In this work, we systematically investigated the structure-activity performance of nanosized Au/CeO_2 and $Au/Ce_{0.9}Fe_{0.1}O_{2-\delta}$ catalysts, along with nanocrystalline CeO_2 and $Ce_{0.9}Fe_{0.1}O_{2-\delta}$ supports, for the oxidation of carbon monoxide and benzylamine. An extensive physicochemical characterization was undertaken using XRD, BET surface area, BJH analysis, TG-DTA, XPS, TEM, Raman, AAS and CHN analyses. XRD studies confirmed the formation of smaller sized $Ce_{0.9}Fe_{0.1}O_{2-\delta}$ nanocrystallites due to the incorporation of Fe^{3+} ions into the CeO_2 lattice. Interestingly, Raman analysis revealed that the addition of Au remarkably improves the structural properties of the supports, evidenced by F_{2g} peak shift and peak broadening, a significant observation in the present work. TEM images revealed the formation of smaller Au particles for $Au/Ce_{0.9}Fe_{0.1}O_{2-\delta}$ (~3.6 nm) compared with Au/CeO_2 (~5.3 nm), attributed to ample oxygen vacancies present on the $Ce_{0.9}Fe_{0.1}O_{2-\delta}$ surface. XPS studies indicated that Au and Fe are present in metallic and +3 oxidation states, respectively, whereas Ce is present in both +4 and +3 oxidation states (confirming redox nature). Activity results showed that the incorporation of Fe outstandingly enhances the efficacy of Au/CeO_2 catalyst for both CO oxidation and benzylamine oxidation. A 50% CO conversion was achieved at ~349 and 330 K for Au/CeO_2 and $Au/Ce_{0.9}Fe_{0.1}O_{2-\delta}$ catalysts, respectively. As well, the $Au/Ce_{0.9}Fe_{0.1}O_{2-\delta}$ catalyst showed ~99% benzylamine conversion with ~100% dibenzylimine selectivity for 7 h reaction time and 403 K temperature, whereas only 81% benzylamine conversion was achieved for the Au/CeO_2 sample under similar conditions. The excellent performance of $Au/Ce_{0.9}Fe_{0.1}O_{2-\delta}$ catalyst is mainly due to the existence of smaller Au particles and improved synergetic effect between the Au and $Ce_{0.9}Fe_{0.1}O_{2-\delta}$ support. It is confirmed that the oxidation efficiency of Au catalysts is highly dependent on the preparation method.

1. Introduction

Carbon monoxide (CO) oxidation is one of the pivotal heterogeneous catalytic reactions because of its inherent scientific interest and enormous industrial importance.[1-4] For instance, catalytic CO oxidation plays an outstanding role in many industrial applications, such as auto-exhaust purification, CO_2 lasers, CO gas sensors, respiratory protection devices, fuel cells, *etc*. As well, the selective oxidation of amines to corresponding imines is a vital functional group transformation in the chemical industry.[5-10] Imines are versatile intermediates for the synthesis of several valuable chemicals, such as amides, chiral amines, hydroxyamines, oxazolidines, and nitrones. Various hazardous stoichiometric oxidants, like N-tert-butylphenylsulfinimidoyl-chloride and 2-iodoxybenzoic acid, along with large amounts of toxic organic solvents are typically used for amine oxidation.[5] However, the use of green O_2 oxidant for the oxidation of amines is essential from the viewpoints of "12th Green Chemistry Principles". Therefore, there is a great challenge to the scientific community to develop efficient heterogeneous catalysts suitable for both CO oxidation and aerobic oxidation of benzylamine.

Among various catalysts investigated, supported gold nanoparticles (Au NPs) are the most promising oxidation catalysts due to their interesting and unusual catalytic properties.[11,12] Bulk gold had long been considered as an 'inert' metal for heterogeneous catalytic reactions. However, the breakthrough findings of Haruta and Hutchings demonstrated that smaller Au NPs dispersed on appropriate metal oxides exhibit remarkable catalytic activity for CO oxidation and acetylene hydrochlorination, respectively.[13,14] Afterward, the use of nanosized Au catalysts has been vividly increased for a large

[a] Inorganic and Physical Chemistry Division, CSIR – Indian Institute of Chemical Technology, Uppal Road, Hyderabad – 500 007, India. E-mail: bmreddy@iict.res.in; mreddyb@yahoo.com; Fax: +91 40 2716 0921; Tel: +91 40 2719 3510

[b] Centre for Advanced Materials and Industrial Chemistry (CAMIC), School of Applied Sciences, RMIT University, Melbourne VIC 3001, Australia. E-mail: suresh.bhargava@rmit.edu.au; Tel: +61 3 9925 2330

†Electronic supplementary information (ESI) available: TEM, TG-DTA, and XPS studies of the catalysts.

number of reactions, including preferential CO oxidation, selective oxidation of alcohols and amines, chemoselective hydrogenation, epoxidation of styrene, water-gas-shift reaction, oxidation of volatile organic compounds, C-C bond formation, *etc*.[11,15-22] The efficiency of Au catalysts highly depends on the Au particle size, the Au oxidation state, the synthesis method, and the choice of support.[11] Particularly, the nature of the support plays a key role in the oxidation reactions by modifying the properties of Au NPs and/or by affecting the O_2 activation.[23,24] Compared to inert metal oxides (e.g., SiO_2, MgO, and Al_2O_3), active metal oxide supports (e.g., CeO_2, TiO_2, and Fe_2O_3) show a beneficial effect in controlling the nucleation, growth, and stabilization of Au NPs, and consequently, an improved performance of the Au catalysts towards the oxidation reactions.

Ceria (CeO_2), a well-known rare earth metal oxide, has proved to be a potential support for Au NP-catalyzed reactions due to its unique structural and redox characteristics.[25-29] Especially, CeO_2 shows a remarkable ability to shift between two oxidation states $Ce^{3+}\leftrightarrow Ce^{4+}$, resulting in generation of ample oxygen vacancies.[26] These oxygen vacancies act as nucleation sites for the dispersion and stabilization of Au and thereby, outstanding catalytic performance of the Au NPs.[25,29,30] It was reported that nanocrystalline CeO_2 with abundant oxygen vacancies enhances the CO oxidation activity of Au NPs compared with that of the conventional CeO_2.[29] Thus, it was believed that, by modifying the structural and textural properties of CeO_2, the catalytic efficiency of Au/CeO_2 can be improved for the oxidation reactions.

Significant efforts have been undertaken to optimize the physiochemical properties of CeO_2 by incorporating the cation dopants into the CeO_2 lattice.[28,32-38] Doping with appropriate cations enhances the textural properties of CeO_2, for example smaller crystallite size and superior specific surface area.[32] Especially, the introduction of trivalent cations (e.g., Fe^{3+}, La^{3+}, Gd^{3+}, Eu^{3+}, Sm^{3+}, *etc*.) into the CeO_2 leads to generation of ample oxygen vacancies attributed to charge compensation mechanism. For example, substitution of Ce^{4+} by M^{3+} (M = metal) results in the generation of an oxygen vacancy for every two M^{3+} dopants to balance the charge in the CeO_2 lattice. Among various dopants used for modifying the CeO_2 properties, Fe is an interesting dopant attributed to its inexpensive, abundantly available, and environmentally harmless, as well its facile reducible nature ($Fe^{3+/2+}$ ~0.77 V).[39,40] Recently, it was proved that the Fe^{3+}-doped CeO_2 sample exhibits high CO oxidation efficiency compared with that of pristine CeO_2.[39] It is therefore expected that the addition of Au to Fe-doped CeO_2 support shows better structure-activity properties for the oxidation reactions compared with the Au/CeO_2 catalyst.

The present work has been undertaken against the above background. In this study, we prepared nanosized Au/CeO_2 and Au/$Ce_{0.9}Fe_{0.1}O_{2-\delta}$ catalysts using homogeneous deposition precipitation method. The efficiency of developed Au catalysts was studied for the oxidation of CO and benzylamine. For comparison, the catalytic efficiency of CeO_2 and CeO_2-Fe_2O_3 supports was also investigated for the oxidation reactions. The physicochemical properties of supports and corresponding Au catalysts were thoroughly analysed using a number of spectroscopic and non-spectroscopic techniques, such as X-ray diffraction (XRD), transmission electron microscopy (TEM), BET surface area, atomic absorption spectroscopy (AAS), Barrett–Joyner–Halenda (BJH) analysis, thermogravimetric-differential thermal analysis (TG–DTA), X-ray photoelectron spectroscopy (XPS), Raman spectroscopy, and carbon, hydrogen & nitrogen (CHN) analysis. The CO oxidation was conducted in a fixed-bed microreactor at atmospheric pressure. The benzylamine oxidation was performed using O_2 as the green oxidant under solvent-free conditions. Great efforts were made to correlate the activity results with the physicochemical properties of the Au catalysts.

2. Experimental

2.1 Catalysts preparation

An economical co-precipitation method was used to prepare nanocrystalline CeO_2-Fe_2O_3 support (Ce:Fe = 9:1) using aq. NH_3 solution (2.5 w/w%) as the precipitant. In a typical procedure, appropriate amounts of $Ce(NO_3)_3{\cdot}6H_2O$ (Aldrich, AR grade) and $Fe(NO_3)_3{\cdot}9H_2O$ (Aldrich, AR grade) were dissolved separately in double distilled water and mixed together. To this mixture solution, the precipitant was added slowly (min. 2 h duration) until the pH of the solution reached to ~8.5. After completion of the precipitation, a thorough washing procedure was performed with double distilled water to remove the anion impurities. The obtained sample was oven dried at 393 K for 12 h followed by calcination at 773 K for 5 h in air at a heating rate of 5 K min^{-1}. Pure CeO_2 was also prepared by adopting the same procedure.

Nanosized Au/CeO_2-Fe_2O_3 catalyst with 1 wt.% Au loading was prepared by means of homogeneous deposition-precipitation method using urea as the precipitant. The required quantities of urea and $HAuCl_4{\cdot}4H_2O$ (urea:Au = 100, molar ratio) were added to the CeO_2-Fe_2O_3 support under mild stirring conditions. The temperature of the reaction mixture was steadily increased to 353 K and then, the stirring was continued for 12 h at the same temperature. Afterward, the suspension was cooled to room temperature, filtered off, and washed with double-distilled water several times until no traces of Cl^- ions were detected by $AgNO_3$ test. Finally, the sample was oven dried at 373 K for 12 h and calcined in air at 573 K for 4 h (1 K/min). The Au/CeO_2 catalyst with 1 wt.% Au loading was also prepared by adopting the same procedure. For convenience, the prepared samples, namely CeO_2, CeO_2-Fe_2O_3, Au/CeO_2, and Au/CeO_2-Fe_2O_3 were referred to as C, CF, AC, and ACF, respectively.

2.2 Catalysts characterization

A Rigaku diffractometer with Cu Kα radiation (0.15418 nm) and a scintillation counter detector was used to obtain the powder X-ray diffraction patterns of the samples. The XRD patterns were scanned in the range of 2θ = 2-80° with a 0.02° step size and using a counting rate of 1 s/step. Powder Diffraction File-International Center for Diffraction Data (PDF-ICDD) was used to identify the XRD phases present in the catalysts. Scherrer equation and standard cubic indexation method were used to estimate the average crystallite size of CeO_2 and its lattice parameter, respectively.

TEM studies were made on a JEOL JEM-2100F instrument equipped with a slow-scan CCD camera and an accelerating voltage of the electron beam 200 kV. The preparation of samples involves sonication in ethanol for 2–5 min, followed by deposition of a drop on the copper grid supporting a perforated carbon film and allowed to dry. The average Au particle size (dTEM) was calculated from the following formula: dTEM = $\Sigma(n_i d_i)/n_i$, where n_i is the number of Au particles of the diameter, d_i. The elemental analysis of the catalysts was performed with the help of AAS analysis using a Spectra AA-220 Spectrophotometer at a wavelength of 242.8 nm. A Mettler Toledo TG-SDTA instrument was used to conduct the TG-DTA analysis of catalysts. The samples were heated from ambient temperature to 1073 K with a heating rate of 10 K min^{-1} under the flow of N_2. N_2- adsorption/desorption isotherms, surface area, pore size, and pore volume were obtained at 77.25 K on a Micromeritics ASAP 2010 instrument. Prior to analysis, the samples were degassed at 423 K for 12 h and flushed with Ar gas for 2 h. CHN analysis was carried out on Vario Micro Cube Elemental analyser.

XPS studies were performed using a Thermo K-5 Alpha XPS instrument at a pressure better than 1×10^{-9} torr to avoid noise in the spectra. The overall energy resolution of the XPS measurement is 1 eV. The general scan and Ce 3d, Fe 2p, Au 4f, and O 1s core level spectra from the respective samples were recorded using Mg Kα radiation (photon energy = 1253.6 eV) at a pass energy of 50 eV and electron take off angle (angle between electron emission direction and surface plane) of 90°. The core level binding energies (BEs) were charge corrected with respect to the adventitious carbon (C 1s) peak at 284.8 eV. The line shape is Gaussian and background is linear fitting. A Horiba JobinYvon HR 800 Raman spectrometer equipped with a liquid-nitrogen cooled charge coupled device (CCD) detector and a confocal microscope was used for obtaining Raman spectra of the samples. The emission line at 638.2 nm from Ar^+ laser (Spectra Physics) was employed for analysis. The wavenumber values reported from the spectra are accurate to within 2 cm^{-1}.

2.3 Catalytic activity studies

2.3.1 CO oxidation

The CO oxidation activity of the Au samples was conducted at atmospheric pressure in the temperature range of 223 to 573 K using a fixed bed quartz micro-reactor. The reaction was carried out by means of 1% CO and 20% O_2 balanced with He gas. Using mass-flow controllers, 100 ml/min of the feed were dosed onto 100 mg of sample (250–355 µm sieve fraction), which equals to W/F = 0.06 g s ml^{-1}. All gas concentrations were monitored with an X-STREAM X2GP gas analyzer (Emerson), which applies non-dispersive IR photometry for CO and CO_2, and a magnetic method for O_2. Prior to CO oxidation, the catalyst was heated to 573 K in 20% O_2 balanced by He gas using a heating ramp of 1 K min^{-1} and kept at the final temperature for 1 h.

2.3.2 Benzylamine oxidation

The liquid-phase oxidation of benzylamine was performed using O_2 as the oxidant under solvent-free conditions. Typically, 0.2 g of catalyst and 0.2 mmol of benzylamine were taken into a 10 ml three-necked flask equipped with a gas inlet and outlet, a reflux condenser, and a thermometer. Then, the reaction mixture was heated to the required temperature and O_2 was bubbled at a rate of 20 ml/min. After completion of the reaction, the liquid products and the catalyst were separated by centrifugation. The products were confirmed by GC–MS equipped with a DB-5 capillary column and a flame ionization detector (FID). Samples were taken periodically during the reaction and analysed by GC equipped with a BP-20 (wax) capillary column and a FID.

3. Results and discussion

3.1 Characterization studies

The XRD patterns of the Au catalysts and ceria-based supports are shown in Fig. 1. All samples exhibited the standard XRD peaks related to fluorite cubic structured CeO_2.[39] The XRD patterns of CeO_2-Fe_2O_3 shifted to higher angle side (i.e., lattice contraction) compared with pristine CeO_2 attributed to partial replacement of Ce^{4+} (0.97 Å) with smaller sized Fe^{3+} (0.68 Å) in CeO_2 lattice.[39] No XRD lines pertaining to Fe_2O_3 were noticed for the CeO_2-Fe_2O_3 sample, indicating the formation of single phase Ce-Fe solid solution. Noticeably, the CeO_2-Fe_2O_3 sample displays broad diffraction peaks compared with bare CeO_2, implying the formation of smaller crystallite sizes of $Ce_{1-x}Fe_xO_{2-\delta}$ oxide (Table 1).

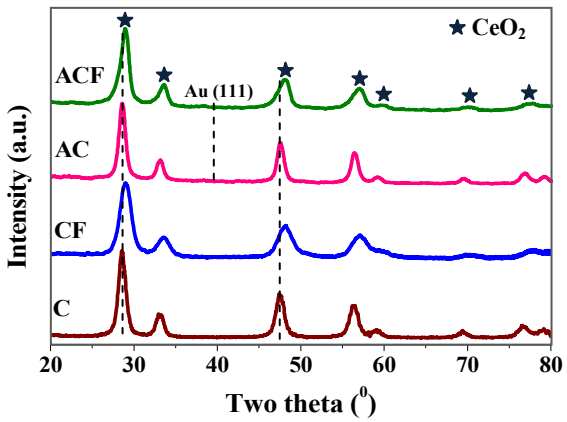

Fig. 1 Powder XRD patterns of CeO_2 (C), CeO_2-Fe_2O_3 (CF), Au/CeO_2 (AC), and Au/CeO_2-Fe_2O_3 (ACF) catalysts.

Table 1 Ceria crystallite size (D), ceria lattice parameter (LP), Au loading, and Au particle size of CeO_2 (C), CeO_2-Fe_2O_3 (CF), Au/CeO_2 (AC), and Au/CeO_2-Fe_2O_3 (ACF) catalysts

Sample	D(nm)[a]	LP (Å)[a]	Au loading (wt.%)[b]	Au particle size (nm)[c]
C	8.9	5.410	–	–
CF	6.7	5.352	–	–
AC	8.7	5.397	0.85	5.3
ACF	6.8	5.354	0.97	3.6

[a] XRD studies. [b] AAS results. [c] TEM images.

Almost identical XRD patterns of ceria supports were obtained after the Au addition. This fascinating observation reveals that the crystalline structure and the average size of the crystalline domain of the ceria supports are well maintained in the Au-containing samples (Table 1).[41] To our surprise, no Au XRD

peaks were found for Au catalysts, which suggest the high dispersion and smaller Au particles (< 5 nm) on the support surface.[41,42] The BET surface area of CeO_2 was considerably increased after Fe-incorporation from 41 to 68 m^2/g (Table 2), in line with crystallite size decrease (Table1).[39] Interestingly, the specific surface area of CeO_2 support was slightly decreased after the Au addition, whereas an improved specific surface area was found for the Au/CeO_2-Fe_2O_3 sample. The obtained specific surface areas of Au/CeO_2 and Au/CeO_2-Fe_2O_3 catalysts were ~39 and 74 m^2/g, respectively. The presence of strong synergetic effect between the Au and CeO_2-Fe_2O_3 support (evidence from Raman analysis, Fig. 4) could be the plausible reason for enhanced specific surface area of the Au/CeO_2-Fe_2O_3 sample.

Table 2 BET surface area, pore size, and pore volume of the CeO_2 (C), CeO_2-Fe_2O_3 (CF), Au/CeO_2 (AC), and Au/CeO_2-Fe_2O_3 (ACF) catalysts

Sample	BET surface area (m^2g^{-1})	Pore size (nm)[a]	Pore volume (cm^3 g^{-1})[a]
C	41	9.818	0.113
CF	68	13.526	0.334
AC	39	3.479	0.066
ACF	74	11.859	0.329

[a] From BJH studies.

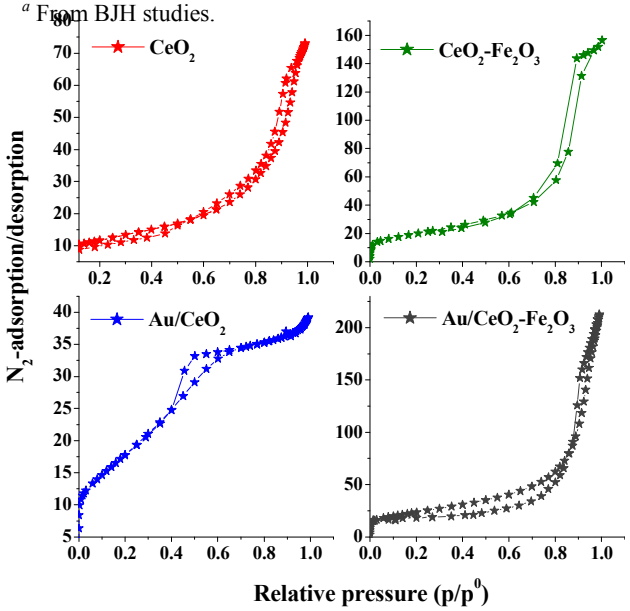

Fig. 2 N_2 adsorption-desorption isotherms of the prepared samples.

Fig. 2 shows the N_2 adsorption-desorption isotherms of the ceria-based supports and corresponding Au catalysts. It was obvious from Fig. 2 that the isotherm of Au/CeO_2 is significantly different compared with that of other samples. Except the Au/CeO_2 sample, all samples exhibit Type IV isotherms with H1-type hysteresis.[43,44] H1-type is often associated with porous materials consisting of well-defined cylindrical-like pore channels. On the other hand, the Au/CeO_2 sample showed typical H_2-type isotherm, in which the distribution of pore size and shape is not well defined and also indicates bottleneck constrictions. As a result, low pore volume and pore size of CeO_2 was found after the addition of Au (Table 2). However, similar changes were not observed in the case of Au/CeO_2-Fe_2O_3 catalyst, probably due to the synergistic interaction between the CeO_2-Fe_2O_3 support and the gold precursors led to the uniform distribution of Au NPs without disturbing the porosity of the CeO_2-Fe_2O_3 support. Atomic absorption spectroscopy results reveal that there was no considerable loss of Au for both Au catalysts. The Au loading of Au/CeO_2 and Au/CeO_2-Fe_2O_3 catalysts were found to be ~0.85 and 0.97%, respectively (Table 1). However, the loss of the Au in the case of Au/CeO_2 sample is more compared with the Au/CeO_2-Fe_2O_3 sample. The presence of oxygen vacancies (nucleation sites for Au particles) on the CeO_2-Fe_2O_3 support might be the reason for observed high Au content in the Au/CeO_2-Fe_2O_3 sample (evidence from Raman analysis, Fig. 4).[25,30] On the other hand, the obtained Ce/Fe ratio (0.89/0.11) is almost close to the calculated value (Ce/Fe = 0.9/0.1), which obviously confirms the stoichiometric atomic concentration. Besides, the chlorine content was found to be very low (<200 ppm) for both Au catalysts.

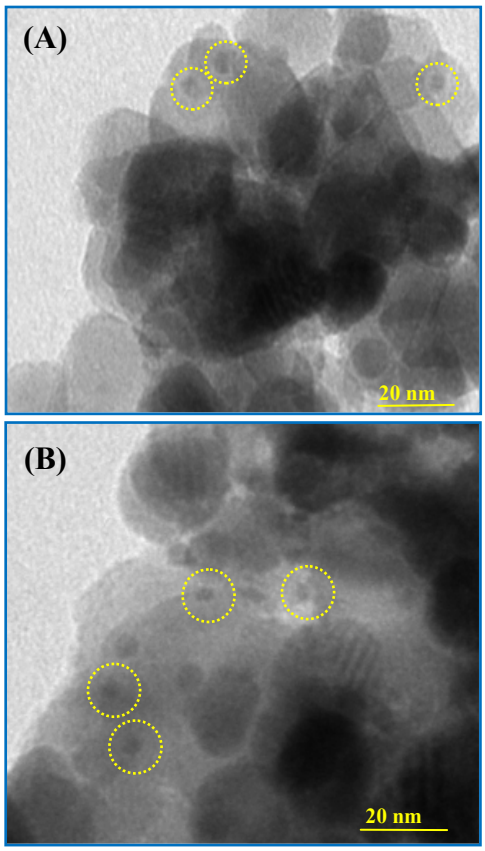

Fig. 3 TEM images of (A) Au/CeO_2 and (B) Au/CeO_2-Fe_2O_3 catalysts.

TEM analysis was performed to know the Au particle size of the Au catalysts (Fig. 3). The Au particles are barely observed from TEM pictures of Au catalysts, which is mainly due to poor contrast between the Au and supports.[45] It was found that the Au/CeO_2-Fe_2O_3 sample contains smaller sized Au NPs with a mean particle size of ~3.6 nm when compared with Au/CeO_2 sample (~5.3 nm). As well, the TEM image of CeO_2-Fe_2O_3 sample evidences the presence of nanosized particles in the range of 10-20 nm (Fig. S1, ESI†). The investigated TG-DTA analysis

of the Au samples shows a major weight loss peak in the range of 373–423 K, corresponding to desorption of water molecules from the catalyst surface (Fig. S2, ESI†). A sharp weight loss peak was also found for the Au/CeO_2 sample at around 823–923 K, attributed to desorption of carbonates held on the catalyst surface. It must be noted here that the appearance of second weight loss peak for the Au/CeO_2-Fe_2O_3 sample is almost negligible.

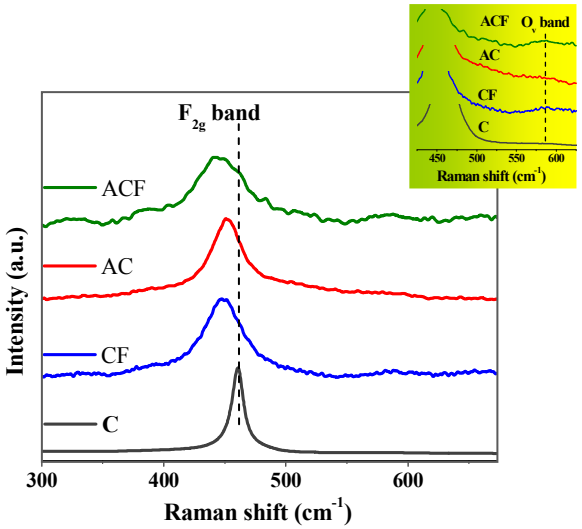

Fig. 4 Raman spectra of CeO_2 (C), CeO_2-Fe_2O_3 (CF), Au/CeO_2 (AC), and Au/CeO_2-Fe_2O_3 (ACF) catalysts.

Raman spectra of the ceria-based supports and corresponding Au catalysts are presented in Fig. 4. A prominent band in the range of ~445-460 cm^{-1} was noticed for all samples, attributed to F_{2g} vibration model of the cubic fluorite type CeO_2, supporting the observations made from the XRD results (Fig. 1).[36] Here also, no characteristic peaks related to Fe_2O_3 were found in the CeO_2-Fe_2O_3 support, which confirm the formation of Fe-doped CeO_2 solid solution.[39] The F_{2g} band of CeO_2-Fe_2O_3 shifts to lower wavenumber side with broadening compared with CeO_2. Indeed, the shifting of the F_{2g} band and its broadness are highly pronounced after the Au addition, which is a remarkable observation in the present study. These unusual structural modifications (F_{2g} band shift and its broadening) depends on several factors, including the ceria particle size, temperature, crystal defects, oxygen vacancies (O_v), phonon confinement, and inhomogeneous strain related to reduced cerium.[46] Usually, vibrations are slow for expanded lattice and rapid for contracted lattice, hence the F_{2g} band shifts to lower and higher wavenumber sides, respectively.[33] Although the CeO_2-Fe_2O_3 support shows lattice contraction (evidence from XRD studies, Table 1 and Fig. 1), it's Raman F_{2g} band shifted to lower wavenumber side. Zhang *et al.* reported that the amount of Fe incorporated into the CeO_2 lattice eventually affects the variation in lattice parameters of the Ce-Fe mixed oxide, thus concentration of oxygen vacancies and Ce^{3+} ions.[47] For small Fe doping amounts (i.e., 1 and 5% of Fe amounts with respect to Ce), a slight lattice expansion can be noticed, attributed to the partial reduction of Ce^{4+} to Ce^{3+}. With the further increase of Fe amount, a gradual decrease in the lattice parameter is observed due to replacement of large amount of Ce^{4+} ions by smaller sized Fe^{3+} ions. The combination of these two factors ultimately leads to smaller lattice parameter for 10% Fe-doped CeO_2 sample accompanied by adequate oxygen vacancies. It is therefore suggested that, despite the smaller lattice parameter, the Ce-Fe support contains ample oxygen vacancies. As stated, a small shoulder at around 600 cm^{-1} was identified for the Ce-Fe support and the corresponding Au catalyst (Fig. 4, inset), which denotes the presence of oxygen vacancies on the sample surface.[24,33] It is generally accepted that the formation of oxygen vacancies induces valence transition of Ce ions in the ceria from +4 to +3, resulting in the formation of active oxygen species as discussed in XPS studies.[48] A meticulous observation of Raman spectra reveals that the shifting of the F_{2g} band is more for Au/CeO_2-Fe_2O_3 when compared with that of the Au/CeO_2 sample, which is mainly due to the existence of strong synergetic effect between the Au and CeO_2-Fe_2O_3 support.[49]

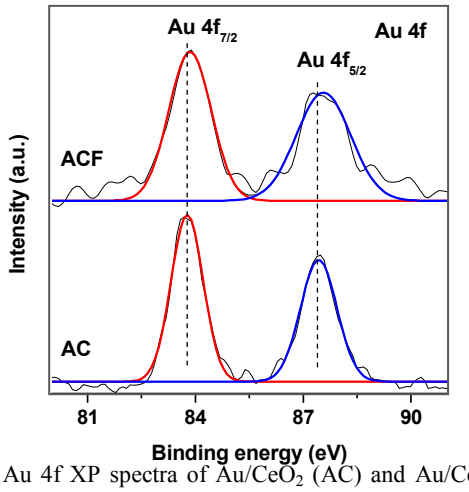

Fig. 5 Au 4f XP spectra of Au/CeO_2 (AC) and Au/CeO_2-Fe_2O_3 (ACF) catalysts.

XPS analysis was performed to know the information about the oxidation states of the elements present in the prepared samples. The estimated binding energies of the Au $4f_{7/2}$, Ce 3d ($u^{///}$), Fe $2p_{3/2}$, and O 1s are summarized in Table 3. Fig. 5 shows the Au 4f XP spectra of the Au/CeO_2 and Au/CeO_2-Fe_2O_3 catalysts. A doublet i.e., Au $4f_{7/2}$ and Au $4f_{5/2}$ with the binding energies of 83.7 ± 0.1 and 87.3 ± 0.1 eV was found for Au/CeO_2 sample, respectively, similar to those of Au/CeO_2-Fe_2O_3 sample at 83.8 ± 0.1 and 87.4 ± 0.1 eV.[24,50] Appearance of these peaks indicates the presence of metallic Au in the prepared Au catalysts. The FWHM values (Au $4f_{7/2}$) of Au/CeO_2 and Au/CeO_2-Fe_2O_3 samples were 1.052 and 1.172 eV, respectively. Interestingly, both Au catalysts show small negative shifts in the Au $4f_{7/2}$ binding energy compared with that of bulk Au (84 eV). The observation of this negative shift indicates the presence of negative charge on the gold, which might be due to electron transfer from the support to Au atoms.[51]

The Ce 3d XP spectra of the samples are shown in Fig. 6. To recognize the valence state features of ceria, the obtained complex spectra have been labelled as per the literature.[33] As shown in Fig. 6, the labels u_0, u, $u^{/}$, $u^{//}$ and $u^{///}$ represent Ce $3d_{3/2}$ ionization. In contrast, the labels v_0, v, $v^{/}$, $v^{//}$ and $v^{///}$ denote Ce $3d_{5/2}$ ionization. Here, the labels v/u, $v^{//}/u^{//}$ and $v^{///}/u^{///}$ arise due to the Ce^{4+} ions and the labels v_0/u_0 and $v^{/}/u^{/}$ show the existence of

Ce^{3+} ions. The presence of Ce^{3+} ions in the prepared samples indicates the redox nature of the ceria. It has been demonstrated that nanosized ceria with ample oxygen vacancies and large amounts of single electron defects (Ce^{3+} ions) exhibits better catalytic performance both as a support and as an active metal phase.[48] As noticed from XRD and Raman studies (Figs. 1 and 4, respectively), the Ce-Fe support shows smaller crystallite size and adequate oxygen vacancies. Therefore, it can be expected that the Au/CeO_2-Fe_2O_3 sample exhibits better catalytic oxidation performance compared with the Au/CeO_2 sample, which is thoroughly discussed in the activity part.

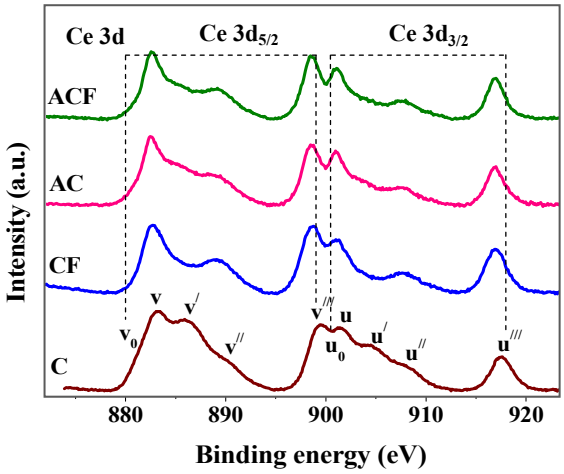

Fig. 6 Ce 3d XPS spectra of CeO_2 (C), CeO_2-Fe_2O_3 (CF), Au/CeO_2 (AC), and Au/CeO_2-Fe_2O_3 (ACF) catalysts.

Table 3 XPS core level binding energies of Au $4f_{7/2}$, O 1s, Ce 3d ($u^{///}$), and Fe $2p_{3/2}$ in CeO_2 (C), CeO_2-Fe_2O_3 (CF), Au/CeO_2 (AC), and Au/CeO_2-Fe_2O_3 (ACF) catalysts

Sample	Au $4f_{7/2}$ (eV)[a]	O 1s (eV)[b]	Ce 3d, $u^{///}$ (eV)[c]	Fe $2p_{3/2}$ (eV)[d]
C	–	530.3	917.5	–
CF	–	529.6	916.9	711.2
AC	83.7	529.3	916.8	–
ACF	83.8	529.3	916.8	–

[a] From Au 4f spectra. [b] From O 1s spectra. [c] From Ce 3d spectra. [d] From Fe 2p spectra.

Fig. 7 shows the O 1s XP spectra of the ceria supports and the corresponding Au catalysts. It is clear from deconvoluted spectra that all samples contain more than one type of oxygen species. The presence of lower energy band for pristine CeO_2 at around 530.3 ± 0.1 eV reveals the ceria lattice oxygen.[36] A broad higher energy band was noticed at 532.6 ± 0.1 eV, which indicates existence of hydroxyl and/or carbonate groups. The peak corresponding to lattice oxygen was shifted towards lower binding energy for the Ce-Fe support in comparison to CeO_2 support (Table 3).[39] Similar peak shifting was also observed for Au-containing samples. These unusual observations indicate labile nature of the lattice oxygen, which might be reason for the generation of oxygen vacancies in the CeO_2-Fe_2O_3 and Au/CeO_2-Fe_2O_3 samples, in line with the Raman results (Fig. 4). As well, the broadening of the ceria lattice oxygen peak is significantly changed after the Au addition to the supports. Au is a highly electronegative metal (2.54 eV), and thereby, it can affects the surrounding environment of Ce-O bond as evidenced from Raman and Ce 3d XPS studies (Figs. 4 and 6, respectively), thus variation in the broadness of the ceria lattice oxygen peak after the Au addition. The FWHM values of O 1s peak (lattice oxygen) of CeO_2, CeO_2-Fe_2O_3, Au/CeO_2 and Au/CeO_2-Fe_2O_3 samples were 1.976, 1.825, 1.198 and 1.242 eV, respectively. The binding energies of Fe $2p_{3/2}$ and Fe $2p_{1/2}$ are found to be ~711.2 ± 0.1 and 724.1 ± 0.1 eV, with two satellite peaks at 718.6 ± 0.1 and 732.4 ± 0.1 eV, respectively (Fig. S3, ESI†).[39,47] Appearance of these binding energy values confirm the presence of Fe^{3+} in the Ce-Fe support.

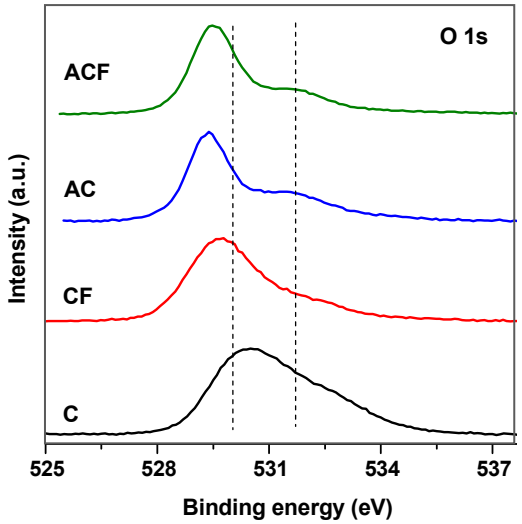

Fig. 7 O 1s XP spectra of CeO_2 (C), CeO_2-Fe_2O_3 (CF), Au/CeO_2 (AC), and Au/CeO_2-Fe_2O_3 (ACF) catalysts.

3.2 Catalytic activity studies

3.2.1 CO oxidation

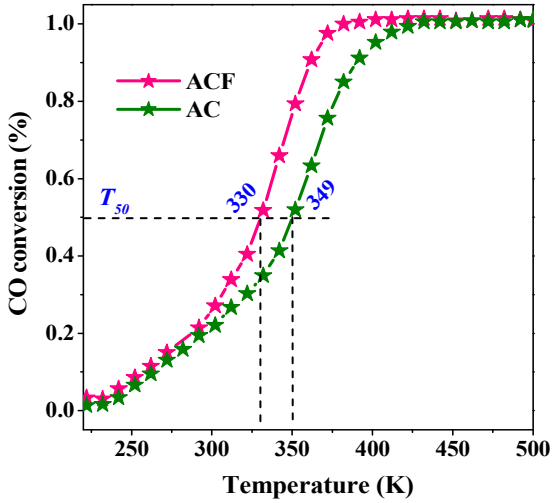

Fig. 8 CO oxidation profiles of Au/CeO_2 (AC) and Au/CeO_2-Fe_2O_3 (ACF) catalysts as a function of temperature.

Fig. 8 shows the CO oxidation profiles of the Au catalysts as a function of temperature. It was found that the CO conversion increases with the temperature for both samples. The Au/CeO_2-Fe_2O_3 catalyst shows 50% CO conversion (T_{50}) at much lower

temperature (T_{50} = ~330 K) compared with the Au/CeO_2 sample (T_{50} = ~349 K). Moreover, the Au/CeO_2-Fe_2O_3 catalyst exhibits 100% CO conversion at ~382 K, whereas the Au/CeO_2 sample shows 100% CO conversion at ~432 K. The outstanding CO oxidation performance of the Au/CeO_2-Fe_2O_3 catalyst is most probably due to the presence of smaller Au NPs and strong synergetic effect between the Au and CeO_2-Fe_2O_3. Our recent study showed that pure CeO_2 and CeO_2-Fe_2O_3 oxides exhibit 50% CO conversion at very high temperatures i.e., ~611 and 480 K, respectively. Hence, the presence of Au is essential for catalyzing the CO oxidation at low temperatures.

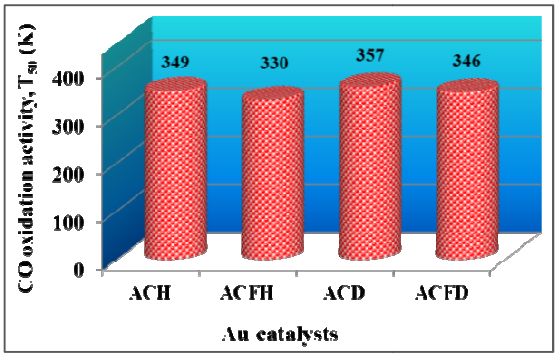

Fig. 9 CO oxidation performance (T_{50}, K) of Au/CeO_2 and Au/CeO_2-Fe_2O_3 catalysts prepared by homogeneous deposition-precipitation (ACH and ACFH) and direct anionic exchange methods (ACD and ACFD), respectively.

Furthermore, we correlated the CO oxidation performance (T_{50} values) of present investigated Au/CeO_2 and Au/CeO_2-Fe_2O_3 catalysts with that of the similar catalysts prepared by direct anionic exchange method (Fig. 9). Details pertaining to the structural characteristics of Au catalysts synthesized by direct anionic exchange could be found elsewhere.[24] It is obvious from Fig. 9 that Au catalysts prepared by homogeneous deposition-precipitation (present work) exhibit superior CO oxidation activity (i.e., low T_{50} values) than that of the direct anionic exchange ones (high T_{50} values). Therefore, the selection of an appropriate preparation method is very important for the synthesis of efficient Au catalysts because different preparation procedures result in different structure-activity properties.

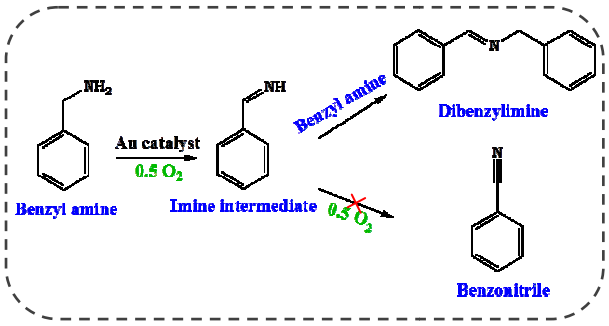

Scheme 1 Reaction pathway for aerobic oxidation of benzylamine over supported Au catalyst.

3.2.2 Benzylamine oxidation

The reaction pathway for the oxidation of benzylamine over Au catalysts is presented in Scheme 1. It was suggested that the complete dehydrogenation of primary amines to yield nitrile is rather difficult over the Au catalysts.[52] Indeed, the oxidation process stops at the intermediate imine stage, which is subsequently reacts with a second molecule of amine to give an intermediate aminal. Finally, the removal of NH_3 from the aminal leads to dibenzylimine product.

The aerobic oxidation of benzylamine over Au catalysts, along with ceria supports was performed and the obtained results are presented in Table 4. The reaction was conducted at 403 K for 4 h using O_2 as the oxidant under solvent-free conditions. Interestingly, the supports also exhibit a considerable catalytic performance in the aerobic oxidation of benzylamine. More interestingly, the incorporation of Fe into the CeO_2 enhances its efficiency towards benzylamine oxidation attributed to structural modifications induced in the Ce-Fe mixed oxide. The achieved benzylamine conversions for CeO_2 and CeO_2-Fe_2O_3 supports were ~18 and 33%, respectively. The activity of the supports was outstandingly improved after the Au addition, which indicates the importance of Au in the oxidation of benzylamine. The benzylamine conversions were found to be ~49 and 65% for Au/CeO_2 and Au/CeO_2-Fe_2O_3 catalysts synthesized by homogeneous deposition precipitation method, respectively. It was clear from Table 4 that the Au catalysts prepared by homogeneous deposition precipitation exhibit high benzylamine conversions compared with that of the direct anionic exchange ones. Despite the catalyst used, the dibenzylimine selectivity was found to be ~99.7–99.9%. We didn't observe any gaseous products, like CO and CO_2 as the present work was performed under liquid phase conditions. Usually, these gaseous products can be observed in the vapour phase reactions at higher temperature conditions.

Table 4 Aerobic oxidation of benzylamine over Au/CeO_2 and Au/CeO_2-Fe_2O_3 catalysts prepared by homogeneous deposition–precipitation (ACH and ACFH) and direct anionic exchange methods (ACD and ACFD), respectively, along with CeO_2 (C) and CeO_2-Fe_2O_3 (CF) supports

Sample	Benzylamine conversion (%)	Selectivity (%)	
		Imine	Nitrile
C	18	99.8	0.2
CF	33	99.9	0.1
ACD	41	99.8	0.2
ACFD	56	99.7	0.3
ACH	49	99.8	0.2
ACFH	65	99.8	0.2

Reaction conditions: reaction time (4 h), reaction temperature (403 K), benzylamine (0.2 mmol), catalyst amount (0.2 g), and O_2 bubbling rate (20 ml/min).

A closer look at the Fig. 10 reveals that the F_{2g} band of Au/CeO_2-Fe_2O_3-homogeneous deposition-precipitation and Au/CeO_2-Fe_2O_3-direct anionic exchange catalysts show red- and blue-shift compared with that of the CeO_2-Fe_2O_3 support, respectively. The observation of the red shift in the case of

Au/CeO_2-Fe_2O_3-homogeneous deposition-precipitation catalyst indicates strong synergetic effect between the Au and CeO_2-Fe_2O_3 and thereby, outstanding performance of the Au/CeO_2-Fe_2O_3-homogeneous deposition-precipitation catalyst for both oxidation reactions compared with that of the Au/CeO_2-Fe_2O_3-direct anionic exchange catalyst.[49] Hence, it is concluded that the oxidation efficiency of Au catalysts strongly depends on the preparation method.

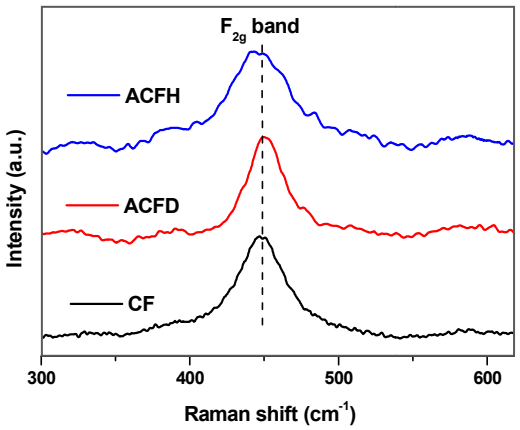

Fig. 10 Raman spectra of CeO_2-Fe_2O_3 (CF), Au/CeO_2-Fe_2O_3-direct anionic exchange (ACFD), and Au/CeO_2-Fe_2O_3-homogeneous deposition-precipitation (ACFH) catalysts.

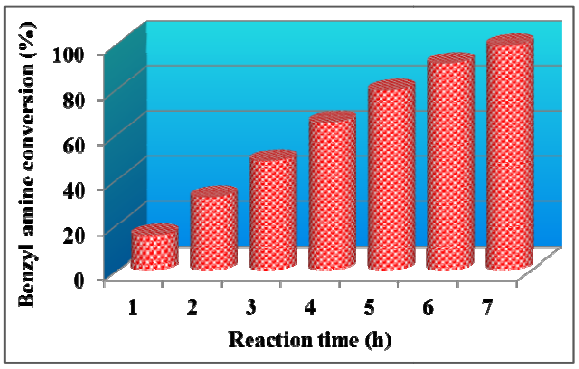

Fig. 11 Influence of reaction time on aerobic oxidation of benzylamine over Au/CeO_2-Fe_2O_3 catalyst. Reaction conditions: reaction temperature (403 K); benzyl alcohol (0.2 mmol); catalyst amount (0.2 g); O_2 bubbling rate (20 ml/min).

The conversion of benzylamine was monitored at different reaction time intervals over the Au/CeO_2-Fe_2O_3 catalyst (Fig. 11). The benzylamine conversion was significantly increased with reaction time, and ~15, 65, and 99% of benzylamine conversions were found for 1, 4, and 7 h of reaction time, respectively. On the other hand, the Au/CeO_2 catalyst exhibits only 81% of benzylamine conversion for 7 h of reaction time. The selectivity of the imine and nitrile were found to be ~99.7–99.9 and 0.1–0.3% at all reaction times. The formation of coke on the catalyst surface, which blocks the active sites, is one of the main reasons for the loss of the catalyst activity in many reactions.[43,53] Especially, in the vapour phase conditions, the coke formation on the catalyst surface is highly feasible. The present study has been carried out in the liquid phase conditions. It is therefore expected that there is no scope of the coke formation on the catalyst surface. It has been also demonstrated that the formation of coke in a liquid-phase oxidation reaction is highly unlikely in the presence of pure O_2.[53] However, to understand the coke formation on the catalyst surface we have performed CHN analysis of the spent Au/CeO_2-Fe_2O_3 catalyst. As expected, no considerable coke formation was observed on the catalyst surface after repeated use.

Conclusions

Nanosized Au/CeO_2 and Au/CeO_2-Fe_2O_3 catalysts were prepared by means of homogeneous deposition precipitation and their catalytic efficiency was studied for two industrially vital oxidation reactions, namely, CO oxidation and benzylamine oxidation. Several characterization techniques were used to understand the physicochemical properties of the catalysts. It was found that the incorporation of Fe into the CeO_2 results in enhanced properties of the final mixed oxides. Interestingly, no Au diffraction peaks were found for Au catalysts due to high dispersion of Au particles on the surface of the ceria supports. Raman measurements revealed that the addition of Au to the ceria supports improve their structural properties. Smaller Au particles were found for the Au/CeO_2-Fe_2O_3 sample compared with the Au/CeO_2 sample. XPS studies showed that Ce is present in the both +4 and +3 oxidation states (redox nature), while Au and Fe are present in the metallic and +3 oxidation state, respectively. It was found that the addition of Fe significantly enhances the performance of the Au/CeO_2 catalyst for both CO oxidation and benzylamine oxidation. The observed 50% CO conversion values for Au/CeO_2 and Au/CeO_2-Fe_2O_3 were ~349 and 330 K, respectively. As well, ~99% benzylamine conversion with almost 100% selectivity to dibenzylimine product was found for the Au/CeO_2-Fe_2O_3 catalyst at 7 h reaction time and 403 K temperature, whereas the Au/CeO_2 shows only 81% benzylamine conversion under identical reaction conditions. The presence of smaller Au particles and strong synergetic effect between the Au and CeO_2-Fe_2O_3 support are found to be key factors for the observed high catalytic efficiency of the Au/CeO_2-Fe_2O_3 sample.

Acknowledgements

P. S. thanks Australian Government, Department of Education for an Endeavour Research Award. The authors duly acknowledge the RMIT Microscopy and Microanalysis Facility (RMMF) for providing access to their instruments used in this study. We greatly acknowledge Prof. Dr. W. Grünert, Rühr University of Bochum, Germany for providing CO oxidation results.

References

1 L. Yang, M. Qia and M. Jin, *CrystEngComm*, 2013, **15**, 2804–2808.
2 W. Song, C. Popa, A. P. J. Jansen and E. J. M. Hensen, *J. Phys. Chem. C*, 2012, **116**, 22904−22915.
3 Y. Zuo, L. Li, X. Huang and G. Li, *Catal. Sci. Technol.*, 2014, **4**, 402–410.
4 R. Liu, N. Gao, F. Zhen, Y. Zhang, L. Mei and X. Zeng,

Chem. Eng. J., 2013, **225**, 245–253.
5 S. Furukawa, A. Suga and T. Komatsu, *Chem. Commun.,* 2014, **50**, 3277–3280.
6 S. Ahmad, K. Gopalaiah, S. N. Chandrudu and R. Nagarajan, *Inorg. Chem.,* 2014, **53**, 2030−2039.
7 L. Aschwanden, T. Mallat, M. Maciejewski, F. Krumeich and A. Baiker, *ChemCatChem*, 2010, **2**, 666–673.
8 L. Aschwanden, T. Mallat, F. Krumeich and A. Baiker, *J. Mol. Catal. A: Chem.,* 2009, **309**, 57–62.
9 L. Tang, H. Sun, Y. Li, Z. Zha and Z. Wang, *Green Chem.,* 2012, **14**, 3423–3428.
10 S. Kodama, J. Yoshida, A. Nomoto, Y. Ueta, S. Yano, M. Ueshima and A. Ogaw, *Tetrahedron Lett*., 2010, **51**, 2450–2452.
11 M. Alhumaimess, Z. Lin, Q. He, L. Lu, N. Dimitratos, N. F. Dummer, M. Conte, S. H. Taylor, J. K. Bartley, C. J. Kiely and G. J. Hutchings, *Chem. Eur. J.,* 2014, **20**, 1701–1710.
12 M. Sankar, E. Nowicka, E. Carter, D. M. Murphy, D. W. Knight, D. Bethell and G. J. Hutchings, *Nat. Commun.,* 2014, **5**, 3332–3337.
13 M. Haruta, N. Yamada, T. Kobayashi and S. Iijima, *J. Catal.,* 1989, **115**, 301–309.
14 G. J. Hutchings, *J. Catal.,* 1985, **96**, 292–295.
15 K. Qian, L. Luo, H. Bao, Q. Hua, Z. Jianga and W. Huang, *Catal. Sci. Technol.,* 2013, **3**, 679–687.
16 A. Corma and P. Serna, *Science,* 2006, **313**, 332–334.
17 A. Abad, P. Concepcion, A. Corma and H. Garcia, *Angew. Chem. Int. Ed.,* 2005, **44**, 4066–4069.
18 A. Corma and H. Garcia, *Chem. Soc. Rev.,* 2008, **37**, 2096–2126.
19 M. Haruta, *Angew. Chem. Int. Ed.,* 2014, **53**, 52–56.
20 J. Huang, T. Takei, H. Ohashi and M. Haruta, *Appl. Catal. A: Gen.,* 2012, **435–436**, 115–122.
21 V. R. Choudhary and D. K. Dumbre, *Appl. Catal. A: Gen.,* 2010, **375**, 252–257.
22 D. K. Dumbre, V. R. Choudhary, N. S. Patil, B. S. Uphade, S. K. Bhargava, *J. Colloid Interf. Sci.,* 2014, **415**, 111–116.
23 C. Tian, S. –H. Chai, D. R. Mullins, X. Zhu, A. Binder, Y. Guo and S. Dai, *Chem. Commun.,* 2013, **49**, 3464–3466.
24 P. Sudarsanam, B. Mallesham, P. S. Reddy, D. Großmann, W. Grünert and B. M. Reddy, *Appl. Catal. B: Environ.,* 2014, **144**, 900–908.
25 H. Y. Kim, H. M. Lee and G. Henkelman, *J. Am. Chem. Soc.,* 2012, **134**, 1560−1570.
26 P. Lakshmanan, L. Delannoy, C. Louis, N. Biona and J. –M. Tatibouët, *Catal. Sci. Technol.,* 2013, **3**, 2918–2925.
27 M. C. I. Bezen, C. Breitkopf, N. El Kolli, J. –M. Krafft, C. Louis and J. A. Lercher, *Chem. Eur. J.,* 2011, **17**, 7095–7104.
28 O. H. Laguna, M. A. Centeno, F. Romero-Sarria and J. A. Odriozola, *Catal. Today,* 2011, **172**, 118–123.
29 P. Petrova, T. Tabakova, G. Munteanu, R. Zanella, M. Tsvetkov and L. Ilieva, *Catal. Commun.,* 2013, **36**, 84–88.
30 N. Ta, J. Liu, S. Chenna, P. A. Crozier, Y. Li, A. Chen and W. Shen, *J. Am. Chem. Soc*., 2012, **134**, 20585−20588.
31 S. Carrettin, P. Concepcion, A. Corma, J. M. L. Nieto and V. F. Puntes, *Angew. Chem., Int. Ed.,* 2004, **43**, 2538−2540.
32 A. V. Thorat, T. Ghoshal, P. Carolan, J. Holmes and M. A. Morris, *J. Phys. Chem. C,* 2014, **118**, 10700–10710.
33 L. Katta, P. Sudarsanam, G. Thrimurthulu and B. M. Reddy, *Appl. Catal. B: Environ.,* 2010, **101**, 101–108.
34 C. Santra, S. Rahman, S. Bojja, O. O. James, D. Sen, S. Maity, A. K. Mohanty, S. Mazumder and B. Chowdhury, *Catal. Sci. Technol.,* 2013, **3**, 360–370.
35 O. H. Laguna, F. R. Sarria, M. A. Centeno and J. A. Odriozol, *J. Catal.,* 2010, **276**, 360–370.
36 K. Kuntaiah, P. Sudarsanam, B. M. Reddy and A. Vinu, *RSC Adv.,* 2013, **3**, 7953–7962.
37 T. Tabakova, L. Ilieva, I. Ivanov, R. Zanella, J. W. Sobczak, W. Lisowski, Z. Kaszkur and D. Andreeva, *Appl. Catal. B: Environ., 2013*, **136–137,** 70–80.
38 L. Katta, P. Sudarsanam, B. Mallesham and B. M. Reddy, *Catal. Sci. Technol.,* 2012, **2**, 995–1004.
39 P. Sudarsanam, B. Mallesham, D. N. Durgasri and B. M. Reddy, *RSC Adv.,* 2014, **4**, 11322–11330.
40 Y. Zuo, X. Huang, L. Li and G. Li, *J. Mater. Chem. A,* 2013, **1**, 374–380.
41 X. Liu, S. Ye, H. –Q. Li, Y. –M. Liu, Y. Cao and K. –N. Fan, *Catal. Sci. Technol.,* 2013, **3**, 3200–3206.
42 F. Cardenas-Lizana, S. Gomez-Quero, N. Perret and M. A. Keane, *Catal. Sci. Technol.,* 2011, **1**, 652–661.
43 B. Mallesham, P. Sudarsanam and B. M. Reddy, *Catal. Sci. Technol.,* 2014, **4**, 803–813.
44 B. Mallesham, P. Sudarsanam, G. Raju and B. M. Reddy, *Green Chem.,* 2013, **15**, 478–489.
45 M. M. Wang, L. He, Y. M. Liu, Y. Cao, H. Y. He and K. N. Fan, *Green Chem.,* 2011, **13**, 602–607.
46 Y. Lee, G. He, A. J. Akey, R. Si, M. Flytzani-Stephanopoulos and I. P. Herman, *J. Am. Chem. Soc.,* 2011, **133**, 12952–12955.
47 Z. Zhang, D. Hana, S. Wei and Y. Zhang, *J. Catal.,* 2010, **276**, 16–23.
48 Y. Liu, B. Liu, Q. Wang, Y. Liu, C. Li, W. Hu, P. Jing, W. Zhao and J. Zhang, *RSC Adv.,* 2014, **4**, 5975–5985.
49 M. Wang, F. Wang, J. Ma, M. Li, Z. Zhang, Y. Wang, X. Zhang and J. Xu, *Chem. Commun.,* 2014, **50**, 292–294.
50 X. Zhang, H. Shi and B. Q. Xu, *J. Catal.,* 2011, **279**, 75–87.
51 M. H. Ab Rahim, Q. He, J. A. Lopez-Sanchez, C. Hammond, N. Dimitratos, M. Sankar, A. F. Carley, C. J. Kiely, D. W. Knight and G. J. Hutchings, *Catal. Sci. Technol.,* 2012, **2**, 1914–1924.
52 M. T. Schumperli, C. Hammond and I. Hermans, *ACS Catal.,* 2012, **2**, 1108–1117.
53 C. D'Agostino, Y. Ryabenkova, P. J. Miedziak, S. H. Taylor, G. J. Hutchings, L. F. Gladdena and M. D. Mantle, *Catal. Sci. Technol.,* 2014, **4**, 1313–1322.